IEEE Access
Multidisciplinary | Rapid Review | Open Access Journal

Received November 5, 2019, accepted November 19, 2019, date of publication November 29, 2019,
date of current version December 13, 2019.

Digital Object Identifier 10.1109/ACCESS.2019.2956830

Design and Optimization of Concentric Tube Robots Based on Surgical Tasks, Anatomical Constraints and Follow-the-Leader Deployment

XING YANG[1], SHUANG SONG[1], LI LIU[2], TINGFANG YAN[3], AND MAX Q.-H. MENG[2], (Fellow, IEEE)

[1]Shenzhen Key Laboratory of Mechanisms and Control in Aerospace, Harbin Institute of Technology, Shenzhen 518055, China
[2]Robotics, Perception and Artificial Intelligence Laboratory, The Chinese University of Hong Kong, Hong Kong
[3]Yuanhua Technology Limited, Shenzhen 518055, China

Corresponding authors: Shuang Song (songshuang@hit.edu.cn) and Li Liu (liliu@cuhk.edu.hk)

This work was supported in part by the National Natural Science Foundation of China under Grant 61803123, in part by the Science and Technology Innovation Committee of Shenzhen under Grant JCYJ20170413110250667, and in part by the Shenzhen Key Laboratory Fund of Mechanisms and Control in Aerospace under Grant ZDSYS201703031002066.

ABSTRACT Many neurological disorders are characterized by the focal and anatomically definable lesions within the brain parenchyma. Traditional treatment may introduce major trauma in neurosurgery and conventional medical devices can only trace straight trajectories. To overcome these problems, a design and optimization method for a patient-specific concentric tube robot (CTR) satisfying the constraints of anatomy, surgical tasks and follow-the-leader (FTL) deployment is proposed in this paper. CTR is a tentacle like continuum robot that can work inside confined and complex biological chambers with the ability of tracking complex 3D trajectories. It consists of pre-curved superplastic tubes with hollow cavities to accommodate the surgical tools. These merits make the CTR well suitable for minimally invasive surgeries. This paper introduces a design framework that utilizes preoperative MRI data to configure patient-specific CTR for single and multiple tasks with the minimum number of tubes. A constant curvature circular arc model is built to solve the problem of inverse kinematics. Two iterative optimization methods for single and multiple tasks are proposed to optimize the parameters of the CTR. Initial waypoints of the CTR are produced based on the FTL deployment. The waypoints are then refined using a Follow Shape Rapidly-exploring Random Tree algorithm (FSRRT) for cases that the initial configurations of the CTR cannot completely satisfy the FTL deployment. Simulations and experiments are carried out on a human brain model to validate the proposed methods. The parameters of CTR including the entire length, curvature, radius angle, number, diameter, arc length and the waypoints are obtained. The errors of the FTL deployment are found to be within 2.1mm.

INDEX TERMS Anatomical constraints, concentric tube robot, follow-the-leader deployment, multi-surgical tasks, patient-specific design and optimization.

I. INTRODUCTION

A wide variety of neurological disorders are characterized by focal and anatomically definable lesions within the brain parenchyma. Such diseases include intracerebral hemorrhage (ICH), brain tumors, stroke, traumatic brain injury, epilepsy, neurodegenerative disorders, and so on. The compartmental or local therapy method is to deliver therapeutic agents directly at or around the desired site [1]. One technique used cannulas or needles to infuse therapeutic agents or auxiliary devices directly into the brain parenchyma [2]. Current cannula placement techniques are limited to follow straight trajectories, which struggle to properly access non-linear targets. Furthermore, the cannulas must be appropriately positioned to avoid critical structures or functional areas [3]. Take the ICH for example which is shown in Fig.1(1a), clinical statistics indicate that if hematoma is larger than 3cm in diameter, it cannot be treated solely with medication, but has to be surgically removed by suction out the semi-coagulated blood to release pressure on brain parenchyma [4]. For those scenarios in which hemorrhage occurs deeply within cerebral cortex, conventional surgical approaches can result in heavy

The associate editor coordinating the review of this manuscript and approving it for publication was Christopher H. T. Lee.

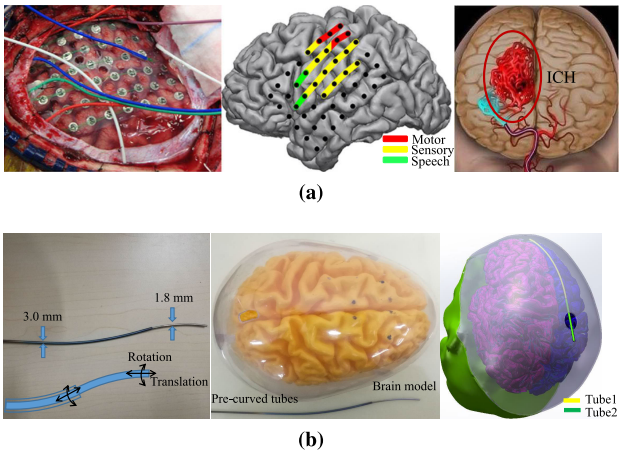

FIGURE 1. **Auxiliary tools applied to neurosurgical minimally invasive surgeries. (a) shows two cases: a neurosurgery case that placing electrodes of ECS for the mapping of functional areas; and a case of ICH. (b) shows a tube pair comprised of two pre-curved superelastic Nitinol tubes that can be rotated and translated with respect to each other. Each tube is controlled by two motors: one is for rotation, and the other for translation. The brain model in (b) is obtained by 3D printing based on the data of human brain. The right figure in (b) is a ideal schematic illustrating the feasibility of employing CTR in neurosurgeries.**

invasion to healthy brain tissues with a large opening of the skull (craniotomy) [4]–[6]. Similarly, for some brain diseases related to motor, sensory and speech function areas the electro-cortical stimulation (ECS) as a golden measurement is used to map brain function areas intraoperativel. However, it is necessary to completely open brain with major trauma (see Fig.1(1a)) [5], [6]. Therefore, design of a dexterous manipulator that has the ability to perform complex 3D trajectories and complete appointed surgical tasks with minimal trauma to healthy brain tissues is urgently needed.

To discretely place electrodes and drugs across different brain areas or remove the hematomas of certain locations through a less invasive entry opening hole, this paper proposes to design patient-specific concentric tube robot(CTR) achieving the purpose of protecting healthy tissues adjacent to lesions as much as possible. CTR is a tentacle-like, vimineous, compact and dexterous robot which can be used in minimally invasive surgery with smaller incisions and scars [7]. It has excellent capabilities of working in confined and complex environment. It can overcome the limitations of straight cannulas to perform non-linear 3D minimally invasive trajectories for flexible percutaneous intracranial navigation [8]–[10]. Fig.1(1b) shows a CTR which is comprised of two circularly pre-curved concentric tubes with cross sections similar to catheters and needles. Tubes are hollow to be integrated with surgical tools, such as biopsy device, drug deliver device, suction pipe and electrodes. Pre-curved tubes are usually made by shape memory alloy (SMA) or superelastic plastics, such as Nitinol or polycaprolactone (PCL) [11]. Nitinol is a novel type of functional material that not only has the shape memory function and superelasticity under large strains, but also has good biocompatibility. PCL is a biodegradable and superelastic polyester that often used for sutures. CTR can be manufactured slenderly with diameter in submillimeters [12]. Fig.1(1b) shows that CTR is moving through the gap of cranial bones and cerebral cortex.

Different from conventional robots composed of rigid links and discrete joints, CTRs are composed of nested pre-curved tubes and the final shape is dependent on combined curvatures. In contract to hyper-redundant continuum robots, such as snake robots which composed of closely connected and independently actuated modules, CTRs possess a smaller degree of freedom that is equal to twice the number of tubes at most. In some interventional surgeries such as the interventions by endoscopes or catheters, surgical tools are passive along their entire length and depend on the contact force with surrounding tissues to guide their movement through body orifices. This interactive force on tissues can result in unwanted and unpredictable damage to healthy tissues. Consequently, stiffness of surgery devices need to be reduced to decrease the interactive force, which could limit tasks that can be performed at distal part. Recent researches showed that CTR can provide an acceptable solution to surgery problems in narrow space [8]–[10], [13]. Nested tubes are capable of actively control motion and force application along their entire length with motors attached to one end of tubes. Furthermore, researches showed that CTR can be designed to extend in the form of follow-the-leader (FTL) deployment [13]–[16]. FTL deployment with no collision to tissues can reduce postoperative complications and contact force, which is an important merit in minimally invasive surgeries.

While CTR is a novel innovation, substantial advancement has been made in formulating fundamental theory and employing this technology in minimally invasive surgery [7], [8], [10], [17]–[23]. Clinical applications involve accessing kidney stones [11], percutaneous beating-heart intracardiac surgery [24], optical biopsy in nasal cavity [25], ENT surgery [25], transnasal surgery [26], and so on. In [4] a design method for CTR was proposed to reach multiple lesion locations using sets of tubes. The method in [10] aimed at searching optimal designs that with minimized robot length and curvature, and stable configuration. A parameterization method for CTR was designed in conjunction with a global search optimization algorithm in [27]. A multi-objective particle swarm optimization algorithm was introduced in the design of CTR with variable length in [28].

Although this technology has obtained great academic and clinical progress, a topic that how to design a patient-specific CTR satisfying neurosurgical requirements, anatomical constraints and follow-the-leader deployment has not received much attention yet, which is of great clinical significance. The design of patient-specific CTR for neurosurgery is of high computational complexity and difficulty. First, each tube has two degrees of freedom and tubes are interactively nested together generating complex shapes. CTR's kinematic model can be derived as the solution to a 3D beam-bending problem with split boundary conditions, but it is complex to be used [10], [29]. Second, each candidate solution needs to be evaluated which involves solving

a collision-free path planning problem. Third, in practical neurosurgery, CTR composed of only one section cannot satisfy most requirements. The design method for multiple subsections is inevitable. Fourth, there are usually many lesion regions to dose with drugs, discretely place small electrodes, or suck hemorrhage in neurosurgeries [5]. Thus, designed CTRs must have the capability of reaching multiple locations. Fifth, a patient-specific CTR for neurosurgery patients, especially for the pediatric patients, should provide secure trajectory to reduce the incidence of postoperative complications. However, this is challenging since FTL deployment also requires appropriate telescopic sequence and parameters of CTR [10], [13]–[15].

Primary contribution of this paper is to propose an effective method to configurate a patient-specific CTR based on neurosurgical tasks, anatomical constraints and FTL deployment with minimum number of tubes. For the purpose of computing parameters of continuous constant curvature subsections, a geometry-based method of estimating continuous circular curves is designed, which also provides an alternative solution to inverse kinematics of CTR. To the best of our knowledge, this is the first paper to include geometry-based kinematics in CTR design process, which will greatly reduce the amount of computation and improve accuracy. A fixed-point infection algorithm is designed to accelerate the process of clearance computation and include surgeons' advice in the process of CTR design. To reduce computational complexity, pure FTL deployment is priorly introduced in configuring parameters of CTR. A novel Follow Shape Rapidly-exploring Random Tree (FSRRT) algorithm is designed as posterior amendment to approximately follow the shape of FTL deployment and produce waypoints considering that parameters of CTR may cannot completely satisfy the conditions of pure FTL deployment.

Rest of the paper is organized as follows. In Section II, the method of design and optimization of CTR is presented. Moreover, simulations and experiments in brain model are shown in Section III. Finally, discussions and conclusions will be drawn in Section IV.

II. METHODS

A. OVERVIEW

CTRs are one type of continuum robot usually manufactured as piecewise constant curvatures or variable and irregular curvatures along its whole body. When tubes are nested together, there are two cases in terms of characterizing the interaction of tubes: dominating stiffness tube pair (In this case, the bending stiffness of one tube or tube pair is much larger than that of the others'. The stiffer tube dominates the curvature of other tubes, thus tubes' shape is determined by the stiffer one.) and balanced stiffness tube pair (In this case, tubes are of similar stiffness, and their original curvatures interact to determine their common combined curvature, which varies with relative rotation of tubes) [17]. In practice, statistics shows that if the stiffness of outer dominating tube/tubes is

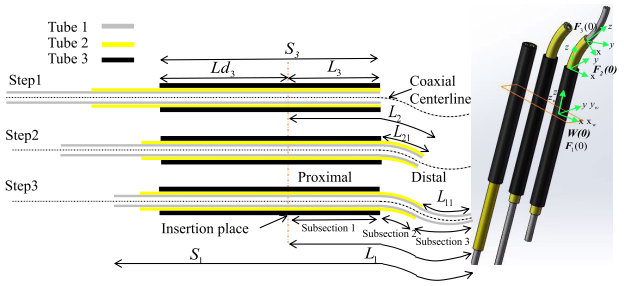

FIGURE 2. FTL deployment of 3 tubes in view of 2D and 3D. Dominating stiffness is chosen here. $W(0)$ is overlapped with $F_1(0)$, where $F_i(0)$ is the base coordination frame of i^{th} subsection. The shape of CTR is composed of 3 subsections.

6 times or larger than that of inner yielded tubes, it can be considered as dominating stiffness tube pair [10].

In this paper, the piecewise constant curvatures model is only considered for its predictable kinematic model and clinical significance, which is favourable for FTL deployment. In latter design and optimization, FTL deployment is firstly introduced to produce robot waypoints, which will bring convenience for kinematic model. To minimize unwanted damage from contact force during surgical operation, FTL deployment is a perfect choice considering the characteristics of CTR. If CTR complies with this movement form, the rest of its continuous body will track the trajectory taken by its head tip, which can be seen in Fig.2. As a consequence, this behavior can reduce total volume occupied by CTR during its whole operation. Moreover, FTL deployment provides a whole path trajectory for neurosurgical tasks. The necessary and sufficient conditions for FTL deployment are fully discussed in [13]–[15].

In addition to surgical requirements, FTL deployment and robot's kinematic model must be took into account during the design of a patient-specific CTR, which becomes a complicated problem. To further simplify the CTR kinematic model without loss of generality, three design guidelines (marked as **G**) are put forward to abide for the purposes of minimally invasive surgery in the remainder of this paper:

a) Initial piecewise constant curvature: Each tube is composed of straight and circular segments. The straight segment is fixed to driven unit for rotation and translation. The circularly pre-curved segment is used for navigation and operation. Tubes' lengths are incremental from outer to inner.
b) Sectionalized dominating stiffness: The stiffness of each telescopic subsection dominates that of all subsections extending from it. The order of extension should execute completely from proximal subsections to distal subsections and the order of retraction is reversed. This will lead to a stable FTL deployment and smaller action space, which is benefit to avoid producing proximal deformation and contact force.
c) Relatively stable curvature: Each telescopic subsection is fixed dominating stiffness (the outermost tube dominates

all inner tubes) or regularly various balanced stiffness (this subsection composed of two tubes and dominates all inner tubes) along its entire length. Thus, the final curvature of combined telescoping subsection can keep constant during one surgical target with piecewise constant curvature design and rational length configuration.

Rules a) and b) enable a CTR to perform as connected circular arcs and extend in the form of FTL deployment. Rules b) and c) keep the proximal part of CTR in a fixed shape during the surgical operation at the distal part. Meanwhile, the two rules qualify CTR with the ability of controllable kinematics and reaching multiple targets. The above rules work together to provide a CTR with three properties: a simple kinematic model, a controllable workspace and the ability to behave as FTL deployment. The constraints of FTL deployment are defined as follows:

$$\Delta_{FTL} = \{\eta_j, \mathbf{G}\}, \quad j = 1, 2, 3...m \tag{1}$$

where η_j is a threshold value of dominating stiffness ratio between dominating tube and inner flexible tubes, m is the number of subsections, $\mathbf{G}$ represents previous design guidelines.

B. SINGLE SUBSECTION ESTIMATING METHOD

In this section a constant curvature arc model will be analyzed to present an geometry-based solution for kinematic problem of CTR. Firstly, for forward kinematics, L_{ij} is employed to notate the insertion length of subsection j of tube i and L_i to notate the total insertion length of tube i, which can be seen in Fig.2. The insertion length of each tube can be designed as:

$$\begin{cases} L_m = L_m \\ L_{m-1} = L_m + L_{(m-1)1} \\ \vdots \\ L_1 = L_2 + L_{11} \end{cases} \tag{2}$$

The total length of each tube S_i is a summation of insertion length L_i and drive part length Ld_i:

$$S_i = L_i + Ld_i, \quad i = 1, 2, 3...n \tag{3}$$

where Ld_i is determined by drive part of CTR and surgery requirements, Ld_i and L_i abide the boundary conditions that $Ld_1 > Ld_2 > \ldots Ld_n > 0$, $L_1 \geq L_2 \geq \ldots L_n \geq 0$ and $S_1 > S_2 > \ldots S_n > 0$. n is the number of tubes. Curvature of tubes can be obtained by equations (4) - (7) [30]:

$$\begin{aligned} \overline{\boldsymbol{u}_i}^{W(0)} &= \boldsymbol{R}_z(\theta_i) \cdot \overline{\boldsymbol{u}_i}^{F_i(0)} \\ &= \boldsymbol{R}_z(\theta_i) \cdot \left[u_{fx}^{F_i(0)}, u_{fy}^{F_i(0)}, u_{fz}^{F_i(0)}\right]^T \end{aligned} \tag{4}$$

$$\boldsymbol{u}_{jf} = \begin{cases} \left(\sum_{i=1}^{k} \boldsymbol{K}_i\right)^{-1} \sum_{i=1}^{k} \boldsymbol{K}_i \overline{\boldsymbol{u}_i}, & \eta \in Balanced \\ \overline{\boldsymbol{u}_d}, & \eta \in Dominating \end{cases} \tag{5}$$

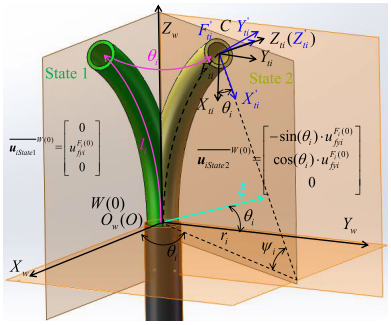

FIGURE 3. Tube coordinate frames and curvatures. State 2 is obtained by a rotation θ_i from state 1 around $+Z_W$-axis. Here we assume that no torsion occurs, thus $u_{fz}^{F_i(0)} = 0$. $\overline{u_{iState1}}^{W(0)}$ and $\overline{u_{iState2}}^{W(0)}$ are the curvatures in State1 and State2 respectively. Magenta lines show the two transformation l_i and θ_i. F_{ti}' and F_{ti} are tip coordination frames of i^{th} subsection.

$$\boldsymbol{K}_i = \begin{bmatrix} E_i I_i & 0 & 0 \\ 0 & E_i I_i & 0 \\ 0 & 0 & J_i G_i \end{bmatrix} \tag{6}$$

$$\|\boldsymbol{u}_{jf}\| = \gamma_j = \frac{1}{r_j} \tag{7}$$

where piecewise coordinate systems based on subsections' constant curvatures are set up, which is shown in Fig.2. As shown in Fig.2 and Fig.3, $W(0)$ is the stationary world frame. $\theta_i \in (0, 2\pi)$ is the rotation angle of tube i, and $\boldsymbol{R}_z(\theta_i) \in \boldsymbol{SO}(3)$ indicates a rotation about $+z$-axis by the angle θ_i. $\overline{\boldsymbol{u}_i}$ is the initial curvature of tube i. $\boldsymbol{u}_{jf}$ is the final combined curvature of subsection j. k is the number of tubes that compros subsection j. $\overline{\boldsymbol{u}_d}$ is the initial curvature of dominating tube or tube pair. As mentioned before, if one subsection belongs to balanced stiffness tube pair, tubes will interact to a combined curvature. Otherwise, if one subsection belongs to dominating stiffness tube pair, tubes will yield to the curvature of dominating tube or tube pair, according to (5). $\boldsymbol{K}_i$ is the bending stiffness of tube i, E_i is the Young modulus of material, I_i is the cross section moment of tube, J_i is the polar moment of inertia, and G_i is the shear modulus. This paper assumes that no torsion occurs, so we set $J_i G_i$=0. r_j is the radius of subsection j, γ_j is equal to the corresponding norm of $\boldsymbol{u}_{jf}$. The diameters of tubes can be derived by:

$$\gamma_j = \frac{1}{E_j I_j} \eta_j \sum_{p=1}^{j-1} E_p I_p \gamma_p \tag{8}$$

Because pure FTL deployment is firstly considered in this paper, the final combined curvatures of subsections behave as:

$$\begin{cases} \|\boldsymbol{u}_{1f}\| = \gamma_1 = c_1 \\ \|\boldsymbol{u}_{2f}\| = \gamma_2 = c_2 \\ \vdots \\ \|\boldsymbol{u}_{mf}\| = \gamma_m = c_m \end{cases} \tag{9}$$

where c_i is the curvature value calculated by inverse kinematics.

Forward kinematic model can be obtained based on the mapping of translation and rotation coordinate systems in robotics. As shown in Fig.3, the translation is l_i and the rotation is θ_i. ψ_i is the central angle corresponding to arc $\widehat{OC}$. $\psi_i * r_i = l_i$. ψ_i describes the rotation from base to tip of i^{th} subsection. For mathematical modeling, translation l_i is applied to i^{th} subsection firstly, thus we get point: $C = \overrightarrow{\boldsymbol{p}} = [r_i(1-\cos\psi_i), 0, r\sin\psi_i]$ and note that this motion includes a rotation: $\boldsymbol{R}_y(\psi_i)$. Secondly, rotation θ_i is applied to i^{th} subsection. As a result, a transformation from base to tip can be calculated:

$$\boldsymbol{T}_{F'_{ti}} = \begin{bmatrix} \boldsymbol{R}_z(\theta_i) & 0 \\ \boldsymbol{0} & 1 \end{bmatrix} \begin{bmatrix} \boldsymbol{R}_y(\psi_i) & \boldsymbol{p} \\ 0 & 1 \end{bmatrix} \tag{10}$$

Note that the X'_{ti}-axis of tip frame in (10) points toward the center of the circle. For the convenience in applications (e.g. when a tool is attached to the tip of the arc), it is helpful to orient the tip frame such that it aligns with the base fame when "slide" along the arc to base with no rotation about the local z-axis [9], which can be obtained by post-multiplying $\boldsymbol{T}_{F'_{ti}}$ by a transformation as follows:

$$\boldsymbol{T}_{ti} = \boldsymbol{T}_W = \boldsymbol{T}_{F'_{ti}} \begin{bmatrix} \boldsymbol{R}_z(-\theta_i) & \boldsymbol{0} \\ \boldsymbol{0} & 1 \end{bmatrix} \tag{11}$$

The transformation matrix for an arbitrary single arc can be then described as:

$$\begin{aligned} &\boldsymbol{T}_j(\boldsymbol{u}_{jf}, \theta_j, \psi_j)_{j=1,2\ldots m} \\ &= \begin{bmatrix} c\theta_j c\psi_j & -c\theta_j & -c\theta_j\psi_j & \dfrac{c\theta_j v\psi_j}{\|u_{jf}\|} \\ s\theta_j c\psi_j & s\theta_j & s\theta_j s\psi_j & \dfrac{s\theta_j v\psi_j}{\|u_{jf}\|} \\ -s\psi_j & 0 & c\psi_j & \dfrac{s\psi_j}{\|u_{jf}\|} \\ 0 & 0 & 0 & 1 \end{bmatrix} Rotz(-\theta_j) \\ &= \begin{bmatrix} 1-c^2\theta_j v\psi_j & -s\theta_j c\theta_j v\psi_j & c\theta_j s\psi_j & -\dfrac{c\theta_j v\psi_j}{\|u_{jf}\|} \\ -s\theta_j c\theta_j v\psi_j & c\psi_j c^2 - \theta_j v\psi_j & s\theta_j s\psi_j & -\dfrac{s\theta_j v\psi_j}{\|u_{jf}\|} \\ -c\theta_j s\psi_j & -s\theta_j s\psi_j & c\psi_j & \dfrac{s\psi_j}{\|u_{jf}\|} \\ 0 & 0 & 0 & 1 \end{bmatrix} \end{aligned} \tag{12}$$

$$\psi_j = l_j \cdot \|\boldsymbol{u}_{jf}\| \tag{13}$$

where $c\theta_j = \cos\theta_j$, $s\theta_j = sin\theta_j$, $c\psi_j = \cos\psi_j$, $s\psi_j = \sin\psi_j$, $v\psi_j = 1-\cos\psi_j$. ψ_j and l_j are central angle and arc length, shown in Fig.3. $Rotz(-\theta_j)$ is a 4×4 homogeneous matrix caused by rotation around $+Z'_{ti}$ axis. The tip frame of CTR can be computed by a concatenation of all subsections:

$$\boldsymbol{W}^{W(0)} = \prod_{j=1}^{m} \boldsymbol{T}_{j(u_{jf},\theta_j,\psi_j)} \tag{14}$$

Generally speaking, the inverse kinematics can be obtained by inverting the forward kinematic formulation. However it is a troublesome because the segmental transformation matrix $\boldsymbol{T}_j$ is complicated and may be irreversible [30]. Thanks to the convenience from FTL deployment, a geometry-based method will be explored to estimate the parameters of single subsection in the following sections.

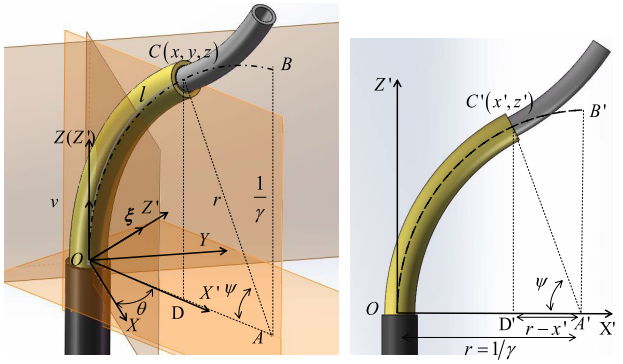

FIGURE 4. Parameterize single subsection. *OXYZ* corresponds to the initial frame $F_i(0)$ and *OX'Y'Z'* corresponds to a temporary frame at the base of one subsection. $\widehat{OC}$ represents the coaxial centerline of this subsection. One of the intermediate nodes O is at origin and the next intermediate node C is located anywhere in 3D space. Before rotating tubes, the center of arc lines in +X-axis. The norm of curvature is the reciprocal of radius based on geometrics. For the convenience of observation, we separate the plane *OAB*, shown on the right.

In clinical neurosurgeries, doctors specify the lesion locations, insertion positions and operation of surgical tools in advance based on CT, MRI or other medical imaging technologies. Fortunately, it is easy to define a circular arc in a closed-form expression in 3D space by given two points' positions and direction at one point, which can be applied to define a subsection arc of CTR. The design problem of single subsection can be then converted to a geometrical problem and solved by robotics and geometrical knowledge. For simplicity, it is assumed that each circular subsection is represented by its coaxial centerline with start point fixed with origin O and insertion direction aligned with $+z$ axis in a right-hand Euclidean space, which is shown in Fig.4. The known inputs are positions of points O, C and the insertion direction v, which map intermediate nodes between different subsections and insertion direction of robot in surgery, respectively. Therefore, configuration of parameters including orientation θ, curvature γ, central angle ψ and arc length l can be solved.

Assuming that position of point C is (x, y, z) and the center point A is in XOY plane. θ can be obtained by:

$$\theta = \tan^{-1}(y/x) \tag{15}$$

In $Z'OX'$ plane, it can be obtained that $x' = \sqrt{x^2+y^2}$ and $z' = z$. Applying Pythagorean theorem in $Rt_{\triangle}A'C'D'$, the curvature can be calculated by:

$$\begin{aligned} \gamma = r^{-1} &= 2x' \Big/ \left(x'^2 + z'^2\right) \\ &= 2\sqrt{x^2+y^2} \Big/ \left(x^2+y^2+z^2\right) \end{aligned} \tag{16}$$

Applying the law of cosines in $Rt_{\triangle}A'C'D'$, we can have $\cos\psi = (r-x')/r = \cos\psi = (\gamma^{-1}-x')/\gamma^{-1}$. Therefore,

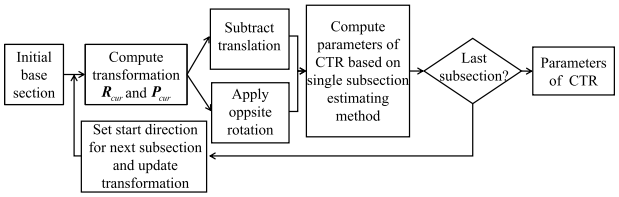

FIGURE 5. The flow chart of continuous multi-subsections estimating method.

results of central angle and arc length can be estimated with the following equation.

$$\psi = \begin{cases} \cos^{-1}\left(1 - \gamma\sqrt{x^2+y^2}\right) & z > 0 \\ 2\pi - \cos^{-1}\left(1 - \gamma\sqrt{x^2+y^2}\right) & z \le 0 \end{cases} \tag{17}$$

$$s = \gamma^{-1}\psi \tag{18}$$

Note that the position of point C is arbitrary. As supplement, this paper disposes special cases based on the position of point C as follows:

a) Case I: $\{C = (0, 0, z)\,|z > 0\}$. This case is handled by representing the centerline of this subsection with a straight line and allocate 0 for θ, z for s. There are no values for γ and ψ.
b) Case II: $\{C = (0, 0, 0)\}$. This case occurs when the arc is a complete circle with arbitrary curvatures or two overlapping points with zero arc length. In order to simplify calculation, we choose the latter one by allocating 0 for θ, s and ψ. There is no value for γ.
c) Case III: $\{C = (0, 0, z)\,|z < 0\}$. This case causes an impossible allocation considering the physical constraints of CTR's subsections whose insertion directions are aligned with the positive $+z$-axis.

As a result, robotic joint variables θ and s can be obtained based on given points and initial direction.

C. CONTINUOUS MULTI-SUBSECTIONS ESTIMATING METHOD

As mentioned in Section I, it is essential to propose a design method for CTR composed of continuous multi-subsections. Fortunately, the constant curvature arc model derived in previous section can be iteratively improved to solve this problem. For each subsection determined by a list of orderly intermediate nodes and a insertion direction, the parameters θ, l, γ and ψ can be calculated depend on previous analysis. In addition, directions at start points are tangent to the adjacent previous subsection for subsections from second to last. The additional work is shown as following and flow chart in Fig.5.

a) Set a base section, which is usually the first subsection;
b) Compute the transformation from base section to current subsection which is determined by the summation of all previous subsections;
c) Subtract the translation caused by previous subsections for subsequent subsection;
d) Apply the opposite rotation of previous subsection to the subsequent subsection;
e) Set the outspread direction of next subsection aligned with $+z$-axis and update transformation for next loop;
f) Compute parameters of this subsection based on previous single subsection estimating method;
g) Repeat steps b)-f) until the last subsection.

The rotation caused by an arbitrary single circular arc in 3D space can be described as rotating about axis $\boldsymbol{\xi} = [-sin\theta, cos\theta, 0]^T$ with an angle ψ [31], which can be seen in Fig.3 and Fig.4. Such that the start point of subsequent subsection is overlapped with the origin point and the tip point of subsequent subsection is adjusted as $\boldsymbol{P}_{lat}$:

$$\begin{aligned} &\boldsymbol{R}_{cur} \\ &= \boldsymbol{R}_{\xi,-\psi}\boldsymbol{R}_{pre} \\ &= \begin{bmatrix} \xi_{xx}v\psi + c\psi & \xi_{yx}v\psi + \xi_z s\psi & \xi_{zx}v\psi - \xi_y s\psi \\ \xi_{xy}v\psi - \xi_z s\psi & \xi_{yy}v\psi + c\psi & \xi_{zy}v\psi + \xi_y s\psi \\ \xi_{xz}v\psi + \xi_z s\psi & \xi_{yz}v\psi - \xi_x s\psi & \xi_{zz}v\psi + c\psi \end{bmatrix} \boldsymbol{R}_{pre} \end{aligned} \tag{19}$$

$$\boldsymbol{P}_{lat} \overset{update}{\longleftarrow} \boldsymbol{R}_{cur}\,(\boldsymbol{P}_{lat} - \boldsymbol{P}_{cur}) \tag{20}$$

where $\xi_{xx} = \xi_x\xi_x$ and $v\psi = 1 - \cos\psi$. $\boldsymbol{P}_{lat}$ is the tip point of subsequent subsection, and $\boldsymbol{P}_{cur}$ is the tip point of current subsection. $\boldsymbol{R}_{\xi,-\psi}$ is the opposite rotation matrix caused by current subsection. $\boldsymbol{R}_{pre}$ is the rotation matrix caused by all previous subsections. Note that $\boldsymbol{R}_{pre}$ needs to be updated by $\boldsymbol{R}_{cur}$ for each loop.

D. DESIGN AND OPTIMIZATION OF CTR FOR SINGLE TASK

Based on the analyses in previous sections, parameters and waypoints of CTR in barrier-free environment can be completely configured. However, anatomical constraints and obstacles of tissues are unavoidable in clinical surgeries. To complete surgical tasks under confined environment, a list of appropriate intermediate nodes that separate different subsections are needed during design of CTR. For CTR's application in surgeries under constrained conditions, the problem of CTR design for a single task point needs to be firstly solved. First of all, a process that establishes virtual surgery environment (notated as $\mathbb{Q}$) for pre-operation simulation shall be set up. In this paper, the initial data of organs and tissues (noted as Ω) are based on MRI data from a human brain model. N-D Convex Hull and Delaunay Triangulation function in MATLAB are employed to cope with the data and 538454 triangles have been produced to describe the brain model as shown in Fig.6, in which a set of interconnected triangles represents the left-brain tissues, which is notated as $\boldsymbol{S}(j)$, and $\Omega = \sum \boldsymbol{S}(j)$.

It is achievable to design a CTR reaching a single task point without constraints of tube number. However, the less number of tubes, the better performance can be achieved considering drive control and manufacture in practice. Therefore, an optimization problem comes that how to obtain an optimal configuration of CTR within confined environment with minimum number of tubes. To solve this problem, we define two

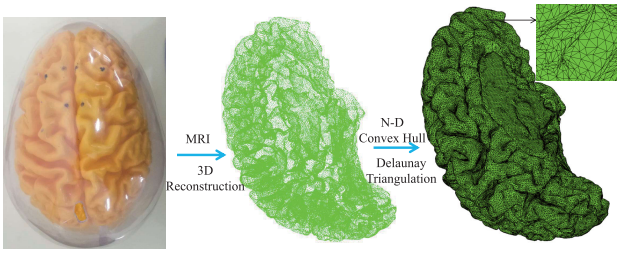

FIGURE 6. Process of representing surgery environment. The left-brain is finally described as 260986 interconnected triangles.

threshold functions $\mathcal{F}_1$, $\mathcal{F}_2$ and two loss functions $\mathcal{F}_3$, $\mathcal{F}_4$ to describe practical constraints.

Function $\mathcal{F}_1$ calculates the number of tubes constituting CTR:

$$\mathcal{F}_1 = n = n_{subs} + n_{balp} = m + n_{balp} \tag{21}$$

where $n_{subs} = m$ is the number of constant curvature subsections, n_{balp} is the number of subsections that are dominated by regularly various balanced stiffness tube pair. Note that each balanced stiffness tube pair needs two interactive tubes and the tube pair together dominates the other tubes in this subsections.

For surgical safety and considering that CTR's slender arm is approximate to a cylinder other than a centerline without volume, function $\mathcal{F}_2$ is established to constrain the minimum distance between centerline of CTR and tissues to avoid penetration of healthy biological organization:

$$\mathcal{F}_2 = \min_{} P_{toS}(\boldsymbol{P}_{CTR}(i), \boldsymbol{S}(j)) \times (i = 1, 2, 3 \cdots N_{CTR}, j = 1, 2, 3 \cdots N_S) \tag{22}$$

where N_s is the number of data sets describing organs and tissues. N_{CTR} is the number of subsections. $\boldsymbol{P}_{CTR}(i)$ is the point set describing CTR's centerline. A point cloud collision detection method $P_{toS}(\boldsymbol{P}_{CTR}(i), \boldsymbol{S}(j))$ is built to calculate the clearances between CTR and tissues based on the distance calculation from one point to triangle in 3D space. The bottom "min" means to search the minimum value of $P_{toS}(\boldsymbol{P}_{CTR}(i), \boldsymbol{S}(j))$. In order to reduce redundant computation in $P_{toS}(\boldsymbol{P}_{CTR}(i), \boldsymbol{S}(j))$, a fixed-point infection algorithm is designed, which is shown in Fig.7. It works as follows: 1)Fetch points in order from base to tip on CTR backbone; 2)Select the nearest point in point cloud of skull based on matrix operations; 3)Outspread the nearest point in step 2) based on structure of triangles, which is built based on the process of representing surgery environment; 4)Compute distance between the fetched point and outspread triangles; 5) Repeat steps 1)-4) until all points on CTR backbone is checked, and output the distances. This algorithm is also employed in latter $\mathcal{F}_4$. At the same time, a margin distance f_{2thr} needs to be allocated for safety, which is no smaller than the maximum radius of tubes. Configurations of

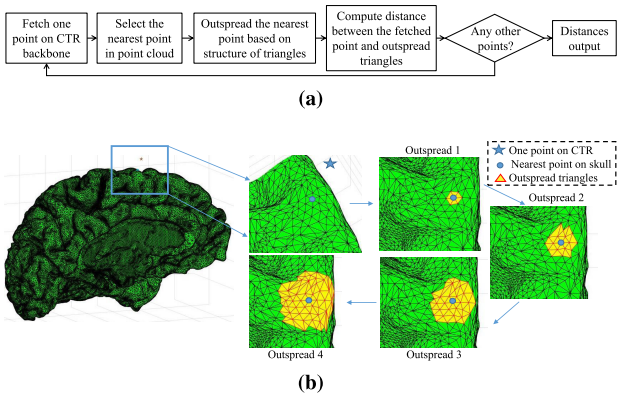

FIGURE 7. Fixed-point infection algorithm. (a) shows the flow chart of fixed-point infection algorithm. (b) shows an example of calculation, where a point (0,0,80)mm in 3D space is marked with star and the nearest point on skull is marked with circle. 4 times of outspread are shown here.

CTR with $\mathcal{F}_2 \geq f_{2thr}$ are put on a candidate list. These clearances are then used to quantify the invasion risk of tissue damage during surgery. The levels of security are described by different colors as shown in Fig.9. This function requires heavy computation due to the mass data of MRI. The distances between CTR's centerline and tissues can be positive or negative. Positive distance means that the corresponding segment is outside tissues and negative distance means that the corresponding segment is penetrated into tissues.

For candidates filtered from function $\mathcal{F}_1$ and $\mathcal{F}_2$, functions $\mathcal{F}_3$ and $\mathcal{F}_4$ are then designed to select optimal configuration. Function $\mathcal{F}_3$ describes the summation of distances between CTR's centerline and tissues, which is estimated by equation (23). It evaluates the security of entire robot arm and needs to be maximized.

$$\mathcal{F}_3 = \sum_{i=1}^{N_{CTR}} \sum_{j=1}^{N_S} P_{toS}(\boldsymbol{P}_{CTR}(i), \boldsymbol{S}(j)) \tag{23}$$

Function $\mathcal{F}_4$ is defined to satisfy special surgical requirements and constraints. For example, surgeons indicate that a surgery operation requires CTR to track some special trajectory points. For some high-risk sensitive areas (marked as $\mathbb{C}_{rs}$), the insertion length within this area must be decreased as much as possible in applications. $\mathbb{C}_{rs}$ is built by previous fixed-point infection algorithm according to surgeons' advice. Therefore, function $\mathcal{F}_4$ defined by (24) is helpful in these cases by penalizing the deviations of waypoints between designed trajectory and designated locations or insertion length in high-risk sensitive area. In addition, some other penalty terms such as the operation direction at tip, curvatures and diameters of tubes can be also involved in optimization function $\mathcal{F}_4$.

$$\mathcal{F}_4 = \sum_{i=1}^{N_\gamma} \alpha_i \left\| \boldsymbol{P}_{a(i)} - \overline{\boldsymbol{P}_{(i)}} \right\| + \sum_{j=1}^{N_{rs}} \beta_j s_{rj} \tag{24}$$

where N_γ is the number of given trajectory points. $\overline{P_{(i)}}$ is the given trajectory point. $P_{a(i)}$ is the nearest point to $\overline{P_{(i)}}$ on CTR backbone. N_{rs} is the number of high-risk sensitive areas. s_{rj} represents the length of CTR in area $\mathbb{C}_{rs}$, which is assessed by $P_{toS}(\boldsymbol{P}_{CTR}(i), \mathbb{C}_{rs})$. α_i and β_j are weightings of the individual subsections. To ensure boundedness of function $\mathcal{F}_4$, the two weightings are constrained as: $\sum_{i=1}^{N_\gamma} \alpha_i = 1$, $\sum_{j=1}^{N_{rs}} \beta_j = 1$.

So far, we have mapped all anatomical constraints (maked as Δ_a: penetration, clearance, special points, and high-risk areas) to functions: $\Delta_a \mapsto \{\mathcal{F}_2, \mathcal{F}_3, \mathcal{F}_4\}$. The final optimization function is defined as follows:

$$\mathcal{F} = \begin{cases} \dfrac{\kappa_3}{\mathcal{F}_3} + \kappa_4 \mathcal{F}_4 & \mathcal{F}_1 \le N_{max},\ and\ \mathcal{F}_2 \le f_{2thr} \\ Inf & others \end{cases} \tag{25}$$

where κ_3 and κ_4 are scale factors. N_{max} is the maximum number of tube decided by drive part. The algorithm to solve design and optimization problem of CTR for single task is shown in Algorithm 1.

Algorithm 1 CTR Design for Single Task

1: Initialize inputs including insertion point, MRI image data and restricted items. Set the initial number of subsections as $m = 1$.
2: Cope the MRI data of surgery environment with the process of representing surgery environment.
3: Divide the surgery environment into several parts (10 parts in this paper) and search intermediate nodes by Mesh Adaptive Direct Search algorithm (MADS).
4: Compute configurations of CTR based on sections II.A - II.C.
5: Compute functions $\mathcal{F}_1$ and $\mathcal{F}_2$, and save the candidates.
6: **if** $\mathcal{F}_1 \le N_{max}$ **then**
7: $m = m + 1$;
8: Go to 3;
9: **else**
10: Compute functions $\mathcal{F}_3$, $\mathcal{F}_4$ and $\mathcal{F}$, record the optimal configuration of CTR.
11: **end if**
12: Stop and export result.

Note that insertion point and surgical restrictions are depend on surgeons' experience. According to the requirements of surgery, the search process of step 3 in Algorithm 1 should be executed within the region of interest (ROI) area (marked as $\mathbb{C}$, which is built depend on the previous fixed-point infection algorithm.) separated by surgeons. Different from $\mathbb{C}_{rs}$, $\mathbb{C}$ is the area which CTR can pass through. In order to avoid the case that traditional Mesh Adaptive Direct Search (MADS) algorithm always traps into local optimal solution, the mesh size is set vary with search steps. On the other hand, search space is averagely divided into several areas in advance in the paper, which means that it is a multi-starts MADS algorithm. Parallel computation is used to accelerate this optimization process in MATLAB.

Algorithm 2 CTR Design for Multiple Tasks

1: Initialize inputs, set $m = 1$.
2: Cope the farthest target with **Algorithm** 1.
3: Set $\gamma_{std(i)} = \gamma_i^1, i = 1, 2, 3 \cdots m$, and take $\gamma_{std(i)}$ into consideration during computing $\mathcal{F}_4$.
4: Cope the remaining targets with **Algorithm** 1, save the best configuration for every target.
5: Compute the mean deviation of curvature $\gamma_{md(i)}$ and the normalized standard deviation $\gamma_{nsv(i)}$ by equations (26)-(28). Compute weighted mean of curvature based on respective arc length by equation (29).
6: Set threshold values γ_{mdthr} and γ_{nsdthr}.
7: **if** $\gamma_{nsv(i)} > \gamma_{nsdthr}$ **then**
8: **if** $\gamma_{md(i)} > \gamma_{mdthr}$ **then**
9: $\gamma_{std(i)}$=$\gamma_{wm(i)}$, $i = 1, 2...m$;
10: Go to 5;
11: **else if** $\mathcal{F}_1 \le N_{max}$ **then**
12: $m = m + 1$;
13: Go to 2;
14: **else**
15: Stop and export no appropriate configuration.
16: **end if**
17: **end if**
18: Compute the configuration of CTR based on $\gamma_{std(i)}$.
19: Check configuration based on $\Delta_a \mapsto \{\mathcal{F}_2, \mathcal{F}_3, \mathcal{F}_4\}$.
20: **if** not satisfy Δ_a **then**
21: go to 2;
22: **end if**
23: Stop and export the configuration.

E. DESIGN AND OPTIMIZATION OF CTR FOR MULTIPLE TASKS

This is an iterative optimization problem where CTR can reach multiple lesion regions with only one tube set. Considering that the farthest task point from insertion position will need longest length of CTR, configuration of the farthest task point is employed to initialize the optimization process of multiple targets based on Algorithm 1. For the reason that curvature is one of key factors for CTR, curvature is taken as the iteration factor for different targets in the paper. γ_i^j is used to notate the candidate curvature of subsection i for target j,$i = 1, 2, 3 \cdots m, j = 1, 2, 3 \cdots N_{mt}$. N_{mt} is the total number of surgery targets. l_i^j notates the arc length. If the number of subsections is unequal for different targets, the last distal subsection is then repeated, but the arc length of the repeated subsection is 0. The algorithm for multiple tasks is defined as Algorithm 2.

$$\gamma_{m(i)} = \frac{1}{N_{mt}} \sum_{j=1}^{N_{mt}} \gamma_i^j, \quad i = 1, 2, 3 \cdots m \tag{26}$$

$$\gamma_{md(i)} = \left| \gamma_{std(i)} - \gamma_{m(i)} \right|, \quad i = 1, 2, 3 \cdots m \tag{27}$$

$$\gamma_{nsv(i)} = \frac{1}{N_{mt}\gamma_{m(i)}} \sum_{j=1}^{N_{mt}} \left(\gamma_i^j - \gamma_{m(i)}\right)^2, \quad i = 1, 2, 3 \cdots m \tag{28}$$

$$\gamma_{wm(i)} = \frac{\sum_{j=1}^{N_{mt}} \left(l_i^j \gamma_i^j\right)}{\sum_{j=1}^{N_{mt}} l_i^j}, \quad j = 1, 2, 3 \cdots N_{mt}, \; i = 1, 2, 3 \cdots m \tag{29}$$

The outermost "if" statement is to check distribution of subsections' curvatures for all targets based on normalized standard deviation. If the deviation is less than a threshold γ_{nsdthr}, then a viable solution has been found. Otherwise, if the mean deviation $\gamma_{md(i)}$ is less enough, standard curvature $\gamma_{std(i)}$ will be replaced with a weighted mean $\gamma_{wm(i)}$ for convergence. If algorithm converges to standard curvature $\gamma_{std(i)}$ (i.e. the mean deviation is less than a threshold γ_{mdthr} because of the operations in previous iteration), meanwhile the distribution is still larger than γ_{nsdthr} and the number of tubes is less than N_{max}, algorithm will add subsections to satisfy the requirements of multiple targets. Another solution is to change this subsection as regularly various balanced stiffness, which will be discussed later in section IV.A. Because curvatures have been iteratively changed, configuration of CTR should be updated and the new configuration must satisfy all constraints.

F. APPROXIMATELY FOLLOW-THE-LEADER DEPLOYMENT

The telescopic sequence of tubes can be controlled, but the bending stiffness determined by materials and parameters calculated by Algorithm 2 cannot always satisfy requirements of FTL deployment, especially for narrow operation environment. For these cases, a novel Follow Shape Rapidly-exploring Random Tree algorithm (FSRRT) based on Rapidly-exploring Random Tree (RRT) is designed to achieve an approximately FTL deployment. The waypoints of CTR is refined at the same time. In order to measure the closeness to FTL deployment, an error metric dependent on CTR's shape is defined:

$$D_s = \sum_{i=1}^{\tau} \left\| \boldsymbol{g}_i - \boldsymbol{e}_i \right\| \tag{30}$$

where $\tau = min\left\{n_g, n_e\right\}$, n_g and n_e are the point volume of $\left\{\boldsymbol{g}_i\right\}$ and $\{\boldsymbol{e}_i\}$. This error metric estimates the deviation of CTR's coaxial centerline to the metric shape produced by FTL deployment. The shape obtained from Algorithm 1 or 2 is designated as the metric shape. The metric shape is described by equidistant points on CTR's centerline, which is denoted by $\left\{\boldsymbol{g}_i\right\}$. Meanwhile, a similar point set $\{\boldsymbol{e}_i\}$ based on kinematics is built. Tip points in the point set are searched by RRT algorithm including collision detection. Points are placed in order from proximal to distal in the two point sets. A threshold value is then set to confine displacement between two point sets:

$$D_{thr} = \lambda_1 \cdot \tau + \lambda_2 \tag{31}$$

where λ_1 and λ_2 are two constants. If the new path point satisfies: $D_s < D_{thr}$, it can then be put in candidate path point tree. Finally, a valid path will be extracted from the candidate tree. The FSRRT algorithm works as following Algorithm 3.

In addition, a preferential region determined by a constant displacement to the metric shape is defined to accelerate the search process. During search process of FSRRT algorithm, sampling is prior to execute in the divided region with a probability of 25%. As a consequence, the sampling is biased to follow metric shape and the search time is expected to be reduced. It looks like that the body of CTR approximately follows the metric shape along its entire length while CTR traces the waypoints searched by FSRRT algorithm. D_{thr} can be an adjustable criterion to control the similarity between metric shape and waypoints planned by FSRRT algorithm.

Algorithm 3 Follow Shape RRT

1: Initialize parameters of RRT based on surgical tasks.
2: Calculate the metric shape $\left\{\boldsymbol{g}_i\right\}$ based on kinematic model and Algorithm 2.
3: Search new path point by RRT.
4: Carry out collision detection along CTR's whole body.
5: **if** collision occurs **then**
6: go back to 3.
7: **end if**
8: Calculate the corresponding CTR shape $\{\boldsymbol{e}_i\}$.
9: Calculate D_s and D_{thr}.
10: **if** $D_s < D_{thr}$ **then**
11: Put the new point in candidate tree;
12: **end if**
13: **if** robot doesn't arrive the target **then**
14: go back to 3.
15: **end if**
16: Extract path from candidate tree. Return the waypoints.

III. EXPERIMENT RESULTS

A. SIMULATIONS FOR ESTIMATING CONTINUOUS CURVES

Simulations and experiments has been carried out to verify the proposed methods. All simulations were executed by MATLAB2018 on a desktop with i7-8700K @ 3.7GHZ. The common goal was to reach surgical tasks points with minimal number of pre-curved tubes. Three simulations were presented to check the validity of inverse kinematic solution for single and multiple subsections shown in Fig.8. For single subsection in Fig.8(5a), the start and end points were $(0, 0, 0)mm$ and $(10, 10, 10)mm$. For combination of three continuous subsections, the intermediate nodes were $(0, 0, 0)mm$, $(0.5, 1.8, 4.6)mm$, $(2.0, 1.1, 8.2)mm$, and $(1, 1, 11)mm$ in Fig.8(5b) and $(0, 0, 0)mm$, $(10, 0, 0)mm$,

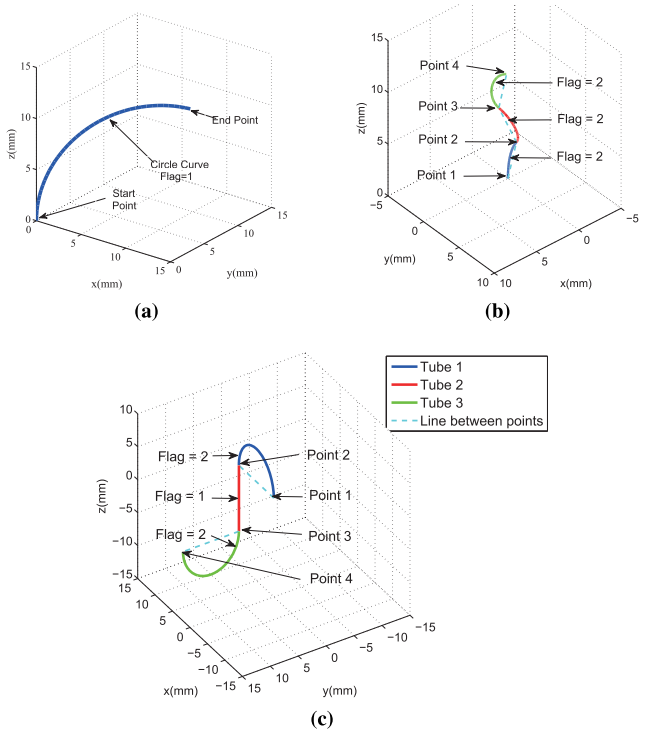

FIGURE 8. Simulations of estimating continuous curves. (a) was a result for single subsection. (b) and (c) were results for multiple subsections. Subsections were distinguished by different colors. For test 2-3, curves were smooth at the intermediate point 2 and point 3. The start points were overlapped with origin; otherwise, we must subtract the corresponding transformations.

TABLE 1. Parameters for continuous curves.

Tests	Test 1	Test 2	Test 3
Rotation θ / radian	0.79	1.30/-1.30/2.60	0/0/1.57
Curvature γ / mm^{-1}	0.09	0.15/0.40/0.64	0.20/-/0.20
Central-Angle ψ / radian	1.91	0.77/1.85/2.54	3.14/-/3.14
Arc-Length s / mm	20.27	5.09/4.59/3.96	15.70/10/15.70
Flag	1	1/1/1	1/2/1

$(10, 0, -10)mm$, $(10, 10, -10)mm$ in Fig.8(5c). The initial direction of first subsection was tangent to $+z$-axis. For remainder subsections, initial directions were tangent to the adjacent previous subsection respectively. Results of tests 1-3 were summarized in Table 1, where notation '$-$' represented no meaningful values. 'Flag 1' represented general cases and 'Flag 2' represented special cases I discussed in section II.B. The cases of II) and III) in section II.B are not shown here, because they have no clinical significance.

B. SIMULATIONS ON 3D BRAIN MODEL

Simulations were carried out on human brain model to verify the design methods in this paper, shown in Fig.9. The data of MRI scanner was represented by three point sets: left-hand brain, right-hand brain and skull. In Fig.9, tubes were represented by different colors. For the purpose of

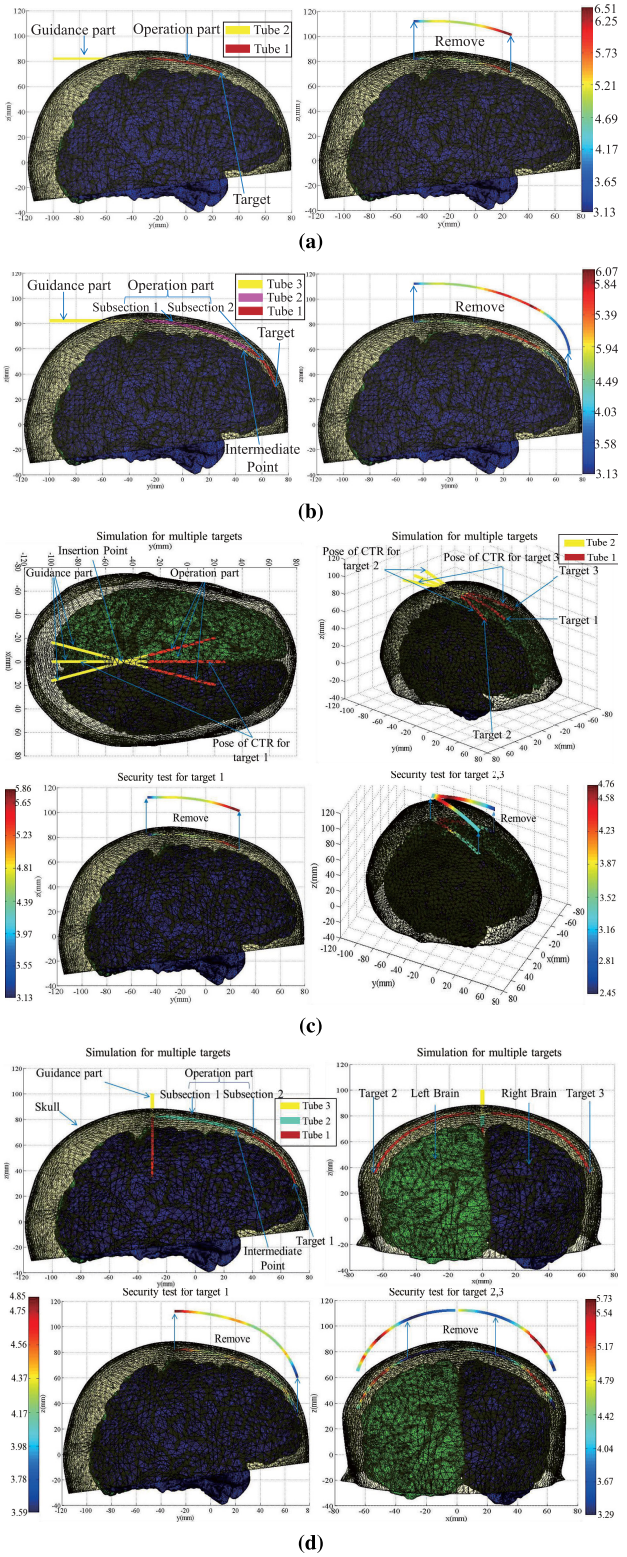

FIGURE 9. Simulations on brain model. (a) and (b) were results of single target and security estimation for test 4 and test 5. (c) and (d) were results of multiple targets and security estimation for test 6 and test 7. The simulation environment was built by the process in section 2.4. The skull was set translucent to show CTR inside model. Color bar represented the distance between CTR and human tissues. For better observing, security estimation was "removed" out of brain model.

TABLE 2. Parameters for test 4,5,6,7.

Tests	Tubes	Do /mm	Di /mm	Curvature radius/mm	Straight length/mm	Curve length/mm	Material
Test4	Tube1	1.8	1.5	156	270	58	Nitinol
	Tube2	2.8	2.0	0	220	-	Nitinol
Test5	Tube1	1.8	1.5	180	210	61	Nitinol
	Tube2	2.8	2.0	64	150	60	Nitinol
	Tube3	4.0	3.0	-	150	-	Stainless Steel
Test6	Tube1	1.8	1.5	156	270	58	Nitinol
	Tube2	2.8	2.0	0	220	-	Nitinol
Test7	Tube1	1.8	1.5	179	211	82	Nitinol
	Tube2	2.8	2.0	64	150	61	Nitinol
	Tube3	4.0	3.0	-	150	-	Stainless Steel

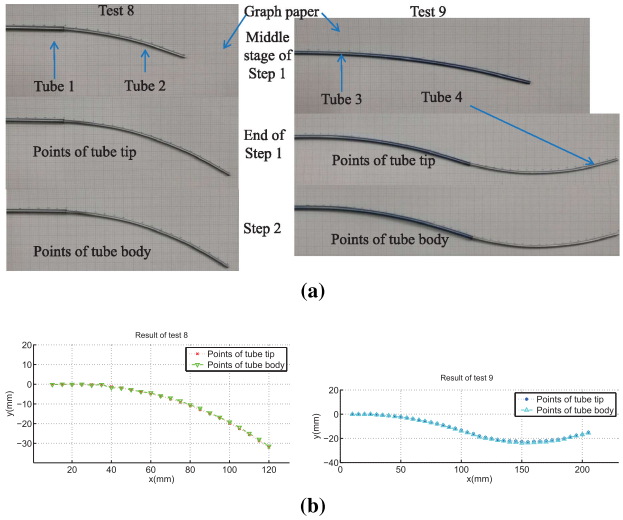

FIGURE 10. Experiments for FTL deployment. (a) Experiments for FTL deployment on graph paper. (b) Results of FTL deployment. In test 8, tube 1 was a straight tube, while tube 2 was a combination of straight and circular parts. In test 9, tube 3 and tube 4 were all combinations of straight and circle parts. The points of tips and CTR body were taken every 5mm in the horizontal direction.

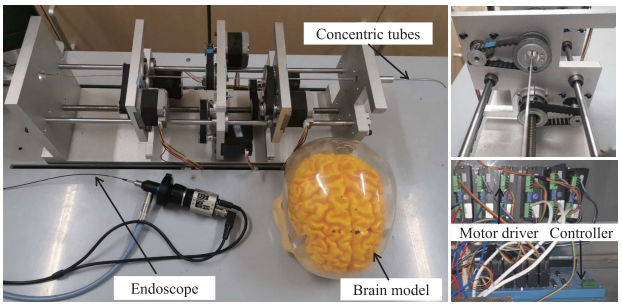

FIGURE 11. Overview of CTR system.

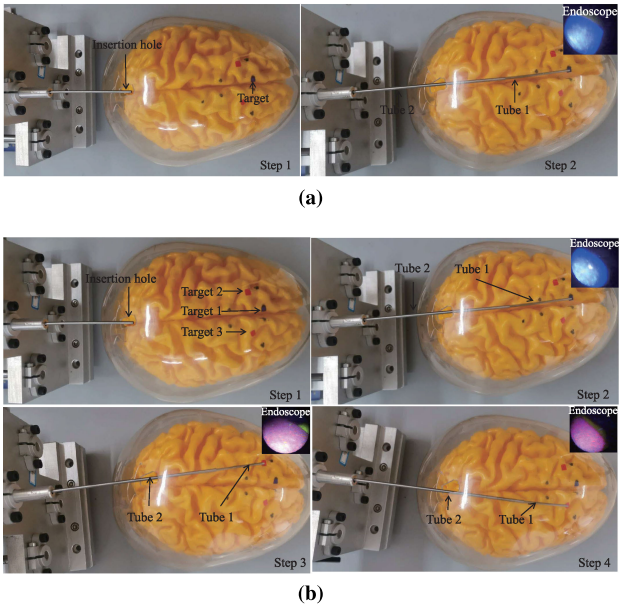

FIGURE 12. Experiments on brain model. (a) test 10 for single target on brain model. (b) test 11 for multiple targets on brain model.

estimating invasion risk of contact force with healthy tissues or penetration, security along entire body of CTR was qualified and levels of warning were presented by different colors. For tests 4-7, the insertion point was $(-47, 0, 82)mm$, which was the center of entry hole on skull. The start point of operation part was $(0, -30, 82)mm$ searched by improved MADS algorithm in MATLAB toolbox, which was a designated trajectory point. A high-risk area was set around the location where the distance between skull and brain was minimum. We set the target point at $(2, 27, 71)mm$ in test 4. For test 5, the target was $(0, 70, 30)mm$. For multiple targets optimization in test 6, the targets were $(2, 27, 71)mm$, $(20, 20, 73)mm$ and $(-20, 20, 73)mm$. Test 7 was another simulation for multiple tasks where targets were $(0, 70, 30)mm$, $(65, -30, 35)mm$ and $(-65, -30, 35)mm$. The results of test 4-7 were recorded in Table 2. Complying with the design guideline of sectionalized dominating stiffness, the outmost tube's material was replaced by stainless steel to reduce the diameter of CTR in test 5 and test 7. In the simulations, the dominating stiffness ratio satisfied $\eta_j > 8$; threshold value f_3thr>2mm; the maximum of tube was 3; $\alpha_i = 1/N_\gamma$, $\beta_j = 1/N_{rs}$, $\kappa_4 = \kappa_5 = 0.5$, $\lambda_1 = 0.04$, $\lambda_2 = 40$.

C. EXPERIMENTS FOR FTL DEPLOYMENT

To verify the designed tubes can perform FTL deployment or approximately FTL deployment, experiments were carried out on graph paper and CTR's trajectories were recorded, which are shown in Fig.10. The experiments included 3 steps:Step 1, record positions of CTR tip during the entire process; Step 2, record positions of CTR body during the entire process; Step 3, calculate deviations between the trajectories of CTR tip and positions of CTR body. The largest displacement error of deployment for two tubes during the whole process was calculated finally, which were 1.4mm for test 8 and 2.1mm for test 9. Taking manufacture errors and concentricity deviations in consideration, the displacement errors of FTL deployment in experiments are acceptable.

D. EXPERIMENTS ON BRAIN MODEL

To verify the proposed methods, a CTR prototype was built shown in Fig.11. The CTR was mainly composed four parts: pre-curved tubes, drive module including motors and motor drivers, transmission module and control module including

a GTS-VB controller of GOOGOLTECH. Results of test 4 and 6 were applied in this section. Test 10 and 11, shown in Fig.12, were corresponded to test 4 and test 6 respectively. Targets were marked by colored labels in these experiments, which could be observed in the view of endoscope when the tip of CTR moved to them. Experiments showed that the designed CTR could reach designated targets under no collision with brain model.

IV. DISCUSSIONS AND CONCLUSION

A. DISCUSSION

In contract to standard robots that are usually designed with unchangeable arms, CTR is relatively easier to change pre-curved tubes for serving different surgical tasks, while it is challenging under constraints of multiple tasks, anatomy and FTL deployment. To address this problem, an optimization method is proposed in this paper. The design method is focused on operation part in this paper, while the guidance part that is usually a straight or right-angle turn tube determined by surgery requirements is integral, e.g. the tube 3 in test 5. There are two reasons for the necessity of guidance part: First, it unifies the insertion hole at a common position for multiple tasks, which can reduce the damage to patients in minimally invasive surgery. Second, the guidance part improves compatibility between the length of different tubes and the length of drives.

For Algorithm 2, there are two alternative solutions to deal with the case that curvature of one subsection still distributes too widely for all targets after changing $\gamma_{std(i)}$: increasing the number of subsections or setting the subsection as regularly various balanced stiffness. These solutions will lead to two types of CTR: comprised of only fixed curvature subsections and comprised of one or more variable curvature subsections. This paper chooses the former type to reduce the complicity of design and control. However, Algorithm 2 cannot satisfy all optimization tasks within constraints of confined environment and tube number. These cases can be solved by equipping multiple sets of tubes and setting many variable curvature subsections, which will be our future work. The design of CTR including multiple arms for complex tasks and tracing continuous boundary curves of lesions in human brain needs to be further investigated.

Different from the methods in [4], [10], [27], [28], the method in this paper aims at producing a single set of tubes meeting multiple tasks' requirements simultaneously with minimum number of tubes. The geometry-based kinematics is designed and firstly included in design process of CTR, which can accelerate optimization process and improve accuracy. Invasion risk of interactive force is quantified based on the clearance between the entire length of CTR and tissues to ensure the safety of surgical operations, which is helpful to access the feasibility and difficulty of surgery. The fixed-point infection algorithm is designed to accelerate the process of clearance computation and include surgeons' advice in the design process of CTR. The novel FSRRT algorithm is introduced as posterior process for special cases to improve the scope of application. Those virtues can improve surgical efficiency and reduce difficulty of operations.

In terms of CTR application in brain surgery, our experimental results on 3D brain model initially demonstrated that it can reach the pre-specified locations on the brain surface with constraints of anatomy and FTL deployment, which was potentially useful to discretely place drugs or electrodes or aspirating hemorrhage across different brain areas with minimal and full customized invasion for the purpose of locating the core brain functional areas. Although simulations and experiments are only tested in brain model, the proposed method can be expanded to apply in other minimally invasive surgeries.

B. CONCLUSION

This paper proposed a design and optimization methodology framework for patient-specific CTR manufacture. The tissues and neurosurgery tasks were prescribed by the sets of interconnected triangles and the 3D coordinate points based on the MRI scanner. Forward kinematics of CTR was analyzed, which was used for shape computing and obstacle avoidance. A constant curvature circular arc model was proposed to solve inverse kinematics. A fixed-point infection algorithm was designed to accelerate the computation and include surgeon's advice in the design process. Algorithms for single and multiple tasks were built to configure the parameters of the CTR. Finally, the FSRRT algorithm was established to achieve approximately the FTL deployment as the post amendment for special cases that configuration of the CTR couldn't completely satisfy the conditions of the pure FTL deployment. The problems in section I can now be successfully solved, which was of great significant in clinical neurosurgery. Experimental results verified the validity of the proposed methods.

REFERENCES

[1] M. Westphal and P. M. Black, "Perspectives of cellular and molecular neurosurgery," *J. Neuro-Oncol.*, vol. 70, no. 2, pp. 255–269, Nov. 2004.

[2] J. A. Engh, D. S. Minhas, D. Kondziolka, and C. N. Riviere, "Percutaneous intracerebral navigation by duty-cycled spinning of flexible bevel-tipped needles," *Neurosurgery*, vol. 67, no. 4, pp. 1117–1123, Oct. 2010.

[3] M. G. Hart, S. J. Price, and J. Suckling, "Functional connectivity networks for preoperative brain mapping in neurosurgery," *J. Neurosurg.*, vol. 126, no. 6, pp. 1941–1950 2017.

[4] J. Granna, Y. Guo, K. D. Weaver, and J. Burgner-Kahrs, "Comparison of optimization algorithms for a tubular aspiration robot for maximum coverage in intracerebral hemorrhage evacuation," *J. Med. Robot. Res.*, vol. 2, no. 1, 2017, Art. no. 1750004.

[5] M. Dey, A. Stadnik, and I. A. Awad, "Thrombolytic evacuation of inracerebral and intraventricular hemorrhage," *Current cardiology reports*, vol. 14, no. 6, pp. 754–760, Dec. 2012.

[6] C. J. van Asch, M. J. Luitse, G. J. Rinkel, I. van der Tweel, A. Algra, and C. J. Klijn, "Incidence, case fatality, and functional outcome of intracerebral haemorrhage over time, according to age, sex, and ethnic origin: A systematic review and meta-analysis," *Lancet Neurol.*, vol. 9, no. 2, pp. 167–176, 2010.

[7] K. Wu, G. Zhu, L. Wu, W. Gao, S. Song, C. M. Lim, and H. Ren, "Safety-enhanced model-free visual servoing for continuum tubular robots through singularity avoidance in confined environments," *IEEE Access*, vol. 7, pp. 21539–21558, 2019.
[8] J. Burgner-Kahrs, D. C. Rucker, and H. Choset, "Continuum robots for medical applications: A survey," *IEEE Trans. Robot.*, vol. 31, no. 6, pp. 1261–1280, Dec. 2015.
[9] R. J. Webster, III, and B. A. Jones, "Design and kinematic modeling of constant curvature continuum robots: A review," *Int. J. Robot. Res.*, vol. 29, no. 13, pp. 1661–1683, 2010.
[10] C. Bergeles, A. H. Gosline, N. V. Vasilyev, P. J. Codd, P. J. del Nido, and P. E. Dupont, "Concentric tube robot design and optimization based on task and anatomical constraints," *IEEE Trans. Robot.*, vol. 31, no. 1, pp. 67–84, Feb. 2015.
[11] T. K. Morimoto, J. J. Cerrolaza, M. H. Hsieh, K. Cleary, A. M. Okamura, and M. G. Linguraru, "Design of patient-specific concentric tube robots using path planning from 3-D ultrasound," in *Proc. 39th Annu. Int. Conf. IEEE Eng. Med. Biol. Soc. (EMBC)*, Jul. 2017, pp. 165–168.
[12] P. Sears and P. Dupont, "A steerable needle technology using curved concentric tubes," in *Proc. IEEE/RSJ Int. Conf. Intell. Robots Syst.*, Oct. 2006, pp. 2850–2856.
[13] Y. Guo, J. Granna, K. Weaver, R. Webster, III, and J. Burgner-Kahrs, "Comparison of optimization algorithms for a tubular aspiration robot for maximum coverage in intracerebral hemorrhage evacuation," in *Proc. Hamyln Symp Med. Robot.*, 2015, pp. 11–12.
[14] H. B. Gilbert and R. J. Webster, "Can concentric tube robots follow the leader?" in *Proc. IEEE Int. Conf. Robot. Automat.*, May 2013, pp. 4881–4887.
[15] H. B. Gilbert, J. Neimat, and R. J. Webster, "Concentric tube robots as steerable needles: Achieving follow-the-leader deployment," *IEEE Trans. Robot.*, vol. 31, no. 2, pp. 246–258, Apr. 2015.
[16] A. Garriga-Casanovas and F. Y. Rodriguez Baena, "Complete follow-the-leader kinematics using concentric tube robots," *Int. J. Robot. Res.*, vol. 37, no. 1, pp. 197–222, Dec. 2018.
[17] P. E. Dupont, J. Lock, B. Itkowitz, and E. Butler, "Design and control of concentric-tube robots," *IEEE Trans. Robot.*, vol. 26, no. 2, pp. 209–225, Apr. 2010.
[18] J. Lock, G. Laing, M. Mahvash, and P. E. Dupont, "Quasistatic modeling of concentric tube robots with external loads," in *Proc. IEEE/RSJ Int. Conf. Intell. Robots Syst.*, Oct. 2010, pp. 2325–2332.
[19] D. C. Rucker, B. A. Jones, and R. J. Webster, III, "A geometrically exact model for externally loaded concentric-tube continuum robots," *IEEE Robot. Automat. Soc.*, vol. 26, no. 5, pp. 769–780, May 2010.
[20] M. Mahvash and P. E. Dupont, "Stiffness control of surgical continuum manipulators," *IEEE Trans. Robot.*, vol. 27, no. 2, pp. 334–345, Apr. 2011.
[21] R. Xu and R. Patel, "A fast torsionally compliant kinematic model of concentric-tube robots," in *Proc. Annu. Int. Conf. IEEE Eng. Med. Biol. Soc.*, Aug./Sep. 2012, pp. 904–907.
[22] K. E. Riojas, R. J. Hendrick, and R. J. Webster, "Can elastic instability be beneficial in concentric tube robots?" *IEEE Robot. Autom. Lett.*, vol. 3, no. 3, pp. 1624–1630, Jul. 2018.
[23] J. Ha, G. Fagogenis, and P. E. Dupont, "Modeling tube clearance and bounding the effect of friction in concentric tube robot kinematics," *IEEE Trans. Robot.*, vol. 35, no. 2, pp. 353–370, Apr. 2018.
[24] A. H. Gosline, N. V. Vasilyev, E. J. Butler, C. Folk, A. Cohen, R. Chen, N. Lang, P. J. Del Nido, and P. E. Dupont, "Percutaneous intracardiac beating-heart surgery using metal mems tissue approximation tools," *The Int. J. Robot. Res.*, vol. 31, no. 9, pp. 1081–1093, May 2012.
[25] C. Girerd, K. Rabenorosoa, P. Rougeot, and P. Renaud, "Towards optical biopsy of olfactory cells using concentric tube robots with follow-the-leader deployment," in *Proc. IEEE/RSJ Int. Conf. Intell. Robots Syst. (IROS)*, Sep. 2017, pp. 5661–5887.
[26] L. Wu, S. Song, K. Wu, C. M. Lin, and H. Ren, "Development of a compact continuum tubular robotic system for nasopharyngeal biopsy," *Med. Biol. Eng. Comput.*, vol. 55, no. 3, pp. 403–417, 2017.
[27] T. Anor, J. R. Madsen, and P. Dupont, "Algorithms for design of continuum robots using the concentric tubes approach: A neurosurgical example," in *Proc. IEEE Int. Conf. Robot. Automat.*, May 2011, pp. 667–673.
[28] J. Granna, A. Nabavi, and J. Burgner-Kahrs, "Computer-assisted planning for a concentric tube robotic system in neurosurgery," *Int. J. Comput. Assist. Radiol. Surg.*, vol. 14, no. 2, pp. 335–344, Feb. 2019.
[29] S. Huang, D. Meng, Y. She, X. Wang, B. Liang, and B. Yuan, "Statics of continuum space manipulators with nonconstant curvature via pseudorigid-body 3r model," *IEEE Access*, vol. 6, pp. 70854–70865, 2018.
[30] P. Sears and P. E. Dupont, "Inverse kinematics of concentric tube steerable needles," in *Proc. IEEE Int. Conf. Robot. Automat.*, Apr. 2007, pp. 1887–1892.
[31] S. Neppalli and B. A. Jones, "Design, construction, and analysis of a continuum robot," in *Proc. IEEE/RSJ Int. Conf. Intell. Robots Syst.*, Oct./Nov. 2007, pp. 1503–1507.

XING YANG received the B.E. degree from the Shandong University of Science and Technology, Shandong, China, in 2012, and the M.E. degree from the North University of China, Taiyuan, China, in 2016, all in mechanical and electronic engineering. He is currently pursuing the Ph.D. degree in mechanical engineering with the Harbin Institute of Technology, Shenzhen. From 2014 to 2016, he was a Joint Student with the Ningbo Institute of Materials Technology and Engineering, Chinese Academy of Sciences. His research field was mobile robot's location and navigation. His current research interests include surgical robotics and continuum robotics.

SHUANG SONG received the B.S. degree in computer science and technology from North Power Electric University, in 2007, the M.S. degree in computer architecture from the Chinese Academy of Sciences, in 2010, and the Ph.D. degree in computer application technology from the University of Chinese Academy of Sciences, China, in 2013. He is currently an Assistant Professor with the Harbin Institute of Technology, Shenzhen, China. His current research interest includes magnetic tracking and actuation for bioengineering applications, such as surgical robots and micro manipulation.

LI LIU received the Ph.D. degree in biomedical engineering from the University of Bern, Switzerland, in 2016. He joined as an Assistant Professor with the Health Science Center, School of Biomedical Engineering, Shenzhen University, in 2016. He is currently a Research Assistant Professor with the Department of Electronic Engineering, The Chinese University of Hong Kong. He has published some 30 peer-reviewed journal and conference papers. His current research interests include computer-assisted surgery, surgical robotics, and AI empowered medical interventions. He was a recipient of the Distinguished Doctorate Dissertation Award from the Best Paper Award of IEEE ICIA, in 2009, the MICCAI Student Travel Award, in 2014, and the Swiss Institute of Computer Assisted Surgery, in 2016. He served as a Publication Chair for many international conferences, including a Publication Chair of IEEE ICIA 2017 and 2018 and a Program Chair of ICIA 2019. He served as a reviewer for several journals and program.

TINGFANG YAN received the B.S. and M.S. degrees from Shandong University, China, in 2011 and 2014, respectively, all in control science and engineering, and the Ph.D. degree in biorobotics from Scuola Superiore Sant'Anna, Pisa, Italy, in 2016. She is currently with the Yuanhua Technology Limited.

MAX Q.-H. MENG received the Ph.D. degree in electrical and computer engineering from the University of Victoria, Canada, in 1992. He was with the Department of Electrical and Computer Engineering, University of Alberta, Canada, as the Director of the Advanced Robotics and Teleoperation (ART) Laboratory and has been an Assistant Professor, since 1994, an Associate Professor, since 1998, and a Professor, since 2000, respectively. He joined The Chinese University of Hong Kong, in 2001, where he is currently a Professor and the Chairman of the Department of Electronic Engineering. He is also an Honorary Chair Professor with the Harbin Institute of Technology, an Honorary Qiushi Chair Professor with Zhejiang University, and the Honorary Dean of the School of Control Science and Engineering, Shandong University, China. He has published more than 600 journal and conference papers and book chapters and led more than 50 funded research projects to completion as PI. His current research interests include robotics, perception, and AI with applications in medicine and services. He has served on a number of international journal editorial boards. He served as an elected member of the AdCom of IEEE RAS. He was a recipient of the IEEE Millennium Medal. He served as the General Chair or Program Chair for many international conferences, including the General Chair of the flagship conferences in robotics: IROS 2005 and ICRA 2021 to be held in Xi'an, in 2021. He served as an Associate VP for Conferences of the IEEE Robotics and Automation Society and a Co-Chair of the Fellow Evaluation Committee. He was a Fellow of the Hong Kong Institution of Engineers and the Canadian Academy of Engineering.